CSIRO Publishing

Publications of the Astronomical Society of Australia

VOLUME 18, 2001

An international journal of astronomy and astrophysics

For editorial enquiries and manuscripts, please contact:
The Editor, PASA,
ATNF, CSIRO,
PO Box 76,
Epping, NSW 1710, Australia
Telephone: +61 2 9372 4590
Fax: +61 2 9372 4310
Email: Michelle.Storey@atnf.csiro.au

For general enquiries and subscriptions, please contact:
CSIRO Publishing
PO Box 1139 (150 Oxford St)
Collingwood, Vic. 3066, Australia
Telephone: +61 3 9662 7666
Fax: +61 3 9662 7555
Email: pasa@publish.csiro.au

Published by CSIRO Publishing
for the Astronomical Society of Australia

www.publish.csiro.au/journals/pasa

Publ. Astron. Soc. Aust., 2001, 18, 421–430

Hydromagnetic Structure of a Neutron Star Accreting at Its Polar Caps

A. Melatos*,[1,2] and E. S. Phinney[2]

[1]School of Physics, University of Melbourne, Parkville, Vic 3010, Australia
a.melatos@physics.unimelb.edu.au
[2]Theoretical Astrophysics, Mail Code 130–33, California Institute of Technology, Pasadena, CA 91125, USA

Received 2001 July 20, accepted 2001 October 10

Abstract: The hydromagnetic structure of a neutron star accreting symmetrically at both magnetic poles is calculated as a function of accreted mass, M_a, starting from a polytropic sphere plus central magnetic dipole ($M_a = 0$) and evolving the configuration through a quasistatic sequence of two-dimensional, Grad–Shafranov equilibria as M_a increases. It is found that the accreted material spreads equatorward under its own weight, compressing the magnetic field into a thin boundary layer and burying it everywhere except in a narrow, equatorial belt. The magnetic dipole moment of the star is given by $\mu = 5.2 \times 10^{24} (B_0/10^{12.5}\,\mathrm{G})^{1.3} (\dot{M}_a/10^{-8}\,M_\odot\,\mathrm{yr}^{-1})^{0.18} (M_a/M_\odot)^{-1.3}\,\mathrm{G\,cm^3}$, and the fractional difference between its principal moments of inertia is given by $\epsilon = 2.1 \times 10^{-5} (B_0/10^{12.5}\,\mathrm{G})^{0.27} (\dot{M}_a/10^{-8}\,M_\odot\,\mathrm{yr}^{-1})^{0.18} (M_a/M_\odot)^{1.7}$, for M_a in the range $10^{-5} \lesssim M_a/M_\odot \lesssim 10^{-1}$, where B_0 is the pre-accretion magnetic field strength, and $\dot{M}_a$ is the accretion rate.

Keywords: accretion, accretion disks — pulsars: general — stars: magnetic fields — stars: neutron

1 Introduction

Neutron stars with a history of mass transfer from a binary companion have systematically lower magnetic dipole moments μ than neutron stars with no accretion history (Bhattacharya & Srinivasan 1995). There are five distinct classes of low-μ objects: (i) binary radio pulsars with a high mass companion, such as another neutron star or a carbon/oxygen white dwarf, which have $\mu = 10^{27.5-28.5}\,\mathrm{G\,cm^3}$; (ii) binary radio pulsars with a low mass companion, such as a helium white dwarf or sub-stellar remnant, which have $\mu = 10^{26-27}\,\mathrm{G\,cm^3}$; (iii) isolated millisecond pulsars (MSPs), which have $\mu = 10^{26-27}\,\mathrm{G\,cm^3}$; (iv) accreting neutron stars in low mass X-ray binaries (LMXBs), the likely progenitors of MSPs (Chakrabarty & Morgan 1998; Wijnands & van der Klis 1998), with $\mu < 10^{27}\,\mathrm{G\,cm^3}$; and (v) some pulsars in globular clusters. In this paper, we restrict attention to low-μ neutron stars in the Galactic disk, because it is hard to accurately infer μ and the rate and duration of accretion for objects in globular clusters, with their complicated kinematics and evolutionary histories.

All the above objects lie to one side of the spin-up line for magnetised equilibrium rotators (Ghosh & Lamb 1979), corrected for accreted mass (Wijers 1997) — qualitative evidence that some kind of accretion induced magnetic field reduction is taking place. Indeed, observations and evolutionary calculations suggest that μ decreases *monotonically* with the mass of accreted material, M_a, down to a floor $\mu_{\min} \approx 10^{26}\,\mathrm{G\,cm^3}$: one finds an inverse correlation between μ and age in high mass X-ray binaries (HMXBs) and binary radio pulsars with high mass companions (Taam & van den Heuvel 1986), and a direct correlation between μ and orbital period P_{orb} in binary radio pulsars with circular orbits and low mass companions (van den Heuvel & Bitzaraki 1995). A simple power law scaling between μ and M_a was proposed by Shibazaki et al. (1989) and subsequently disputed by Wijers (1997). It is clear that μ does not diminish spontaneously in the absence of accretion, as shown by the existence of MSPs with cold, and therefore old, white dwarf companions (Kulkarni 1986), cyclotron-line measurements in LMXBs of known age (Verbunt, Wijers, & Burm 1990), population syntheses of isolated radio pulsars with no accretion history, incorporating survey selection effects (Bhattacharya et al. 1992; Hartman et al. 1997), and calculations of the Ohmic decay time in the crust of a neutron star (Sang & Chanmugam 1987; Urpin & Muslimov 1992; Konar & Bhattacharya 1998).

Three distinct mechanisms of accretion-induced field reduction have been canvassed in the literature to date: accelerated Ohmic decay, vortex–fluxoid interactions, and magnetic screening or burial. Accelerated Ohmic decay occurs when the electrical conductivity of the crust is substantially reduced by accretion-induced heating before the crust sinks under the weight of the overburden and assimilates into the superconducting core of the star (Urpin & Geppert 1995; Urpin & Konenkov 1997; Konar & Bhattacharya 1997, 1998). When applied to LMXBs and HMXBs, including both the propeller and Roche-contact phases of mass transfer, the mechanism reproduces the observed correlation between μ and P_{orb} (Konar & Bhattacharya 1998) and predicts a populous tail of MSPs with rotation periods $P < 1.5$ ms (Possenti et al. 1998). Sengupta (1998) considered general relativistic corrections.

* Also at: Department of Astronomy, 601 Campbell Hall, University of California, Berkeley, CA 94720, USA.

10.1071/AS01056 1323-3580/01/04421$05.00

Neutron vortices and proton fluxoids in the superfluid, superconducting core of a neutron star are thought to interact via Magnus and spin-polarisation forces (Muslimov & Tsygan 1985; Srinivasan et al. 1990; Bhattacharya & Srinivasan 1995). When the star spins down during the propeller phase of accretion, vortices and fluxoids migrate together out of the core and into the heated crust, where there is Ohmic decay (Srinivasan et al. 1990). A high concentration of impurities is needed to attain $\mu_{\min}$ (Konar & Bhattacharya 1999). The vortex–fluxoid interaction may also exert stresses that crack the crust into tectonic plates which shuffle over the surface with magnetic field lines anchored to them (Ruderman 1991a,b; Cheng & Dai 1997), altering μ and forcing the rotation and magnetic axes of MSPs to (counter) align (van den Heuvel & Bitzaraki 1995; Chen, Ruderman, & Zhu 1998).

Magnetic screening takes place when the currents generating the original magnetic field of the star are partially neutralised by crustal currents induced by accretion. Neutralising currents can arise from an inverse thermoelectric battery (Blondin & Freese 1986; cf. Blandford, Applegate, & Hernquist 1983), or if the accretion flow breaks up into diamagnetic blobs that strike the polar caps (Arons & Lea 1980; Zhang, Wu, & Yang 1994; Burderi, King, & Wynn 1996); the latter mechanism was invoked by Burderi et al. (1996) to account for the discrepancy between the spin-down age of PSR J1012+5307 and the cooling age of its white dwarf companion. Neutralising currents can also be induced by burying the field under a spherical accretion flow (Romani 1990, 1993; Toropin et al. 1999) or a flow channelled onto the polar caps (Blandford, de Campli, & Königl 1979; Hameury et al. 1983; Brown & Bildsten 1998; Cheng & Zhang 1998; Sahrling 1998; Litwin, Brown, & Rosner 2001), perhaps in tandem with accelerated Ohmic decay (Romani 1990, 1993; Konar & Bhattacharya 1997, 1998; Sahrling 1998; Cumming, Zweibel, & Bildsten 2001).

In this paper, we extend previous treatments of magnetic burial in three directions: (i) we allow explicitly for equatorward spreading of accreted material and frozen-in magnetic flux, so that high-order magnetic multipoles can develop; (ii) we consider realistic amounts of accreted mass, $10^{-5}M_\odot \lesssim M_a \lesssim 10^{-1}M_\odot$; and (iii) we calculate the hydromagnetic structure of the star self-consistently by solving simultaneously for the density and magnetic field under the action of gravity and the Lorentz force. Previous treatments either prescribed a dipolar magnetic field and spherically symmetric density profile at all stages of accretion (Romani 1990, 1993; Konar & Bhattacharya 1997, 1998), or else permitted equatorward spreading in principle but did not evolve the field to its ultimate, highly distorted state because of numerical difficulties, instead stopping at $M_a \lesssim 10^{-10}M_\odot$ (Hameury et al. 1983; Brown & Bildsten 1998; Litwin et al. 2001). Some physics that appears in earlier works is intentionally neglected in this paper. Our model star is taken to be perfectly conducting; Ohmic decay is not incorporated self-consistently, though its effect is estimated semiquantitatively (cf. Romani 1990, 1993; Urpin & Geppert 1995; Urpin & Konenkov 1997; Konar & Bhattacharya 1997, 1998). We also neglect elastic stresses in the crust (cf. Romani 1990, 1993; Cheng & Zhang 1998).

The paper is structured as follows. In Section 2 and Appendix A, the theory of equatorward hydromagnetic spreading is formalised and then solved by a boundary layer method to obtain the magnetic dipole and mass quadrupole moments of the star as a function of M_a. In Section 3, processes that may limit or disrupt equatorward spreading, such as Ohmic dissipation and hydromagnetic instabilities, are identified and briefly discussed. In a forthcoming paper, we will test the theoretical μ versus M_a relation derived here — which involves just two unknown parameters, the accretion rate $\dot{M}_a$ and the initial magnetic field B_0 — against observational data for different kinds of low-μ neutron stars. We will also calculate the amplitude of gravitational waves emitted by the rotating mass quadrupole. Preliminary estimates suggest that the signal from objects with $M_a \gtrsim 10^{-1}M_\odot$ may be detectable by gravitational wave interferometers under construction (Melatos & Phinney 2000).

2 Theory of Equatorward Hydromagnetic Spreading

In this section, we analyse the evolution of the magnetic field of a neutron star accreting symmetrically at its magnetic poles, as it passes through a quasistatic sequence of hydromagnetic equilibria, from a dipole to an equatorially flaring, tutu-like configuration. A qualitative discussion is given in Section 2.1 to motivate the quantitative theory that follows. We write down the equation of hydromagnetic force balance governing each equilibrium state (Section 2.2), solve it analytically by an approximate boundary layer technique (Section 2.3), and compute the magnetic dipole and mass quadrupole moments of the star (Sections 2.4–2.6).

2.1 Formation of an Equatorial Magnetic Tutu: A Qualitative Picture

Prior to accretion, a neutron star in hydromagnetic equilibrium can be idealised as a spherical, Lane–Emden polytrope threaded by a dipolar magnetic field sustained by point currents at the centre of the star. Let the mass, radius, and polar magnetic field strength of the star be M_*, R_*, and B_0 respectively. We consider accretion onto this initial configuration from a disk situated in the plane of the magnetic equator (Ghosh & Lamb 1979). Accreting material is constrained to flow to the stellar surface along polar magnetic field lines that close outside the inner disk boundary, at radius R_a. North–south symmetry is assumed for simplicity.

During the early stages of accretion, material accumulates on the polar cap, forming a mountain confined magnetically inside the polar flux tube. The distribution of matter and magnetic flux in the mountain can be calculated exactly by Grad–Shafranov methods (Uchida & Low 1981; Hameury et al. 1983; Brown & Bildsten 1998;

https://doi.org/10.1071/AS01056

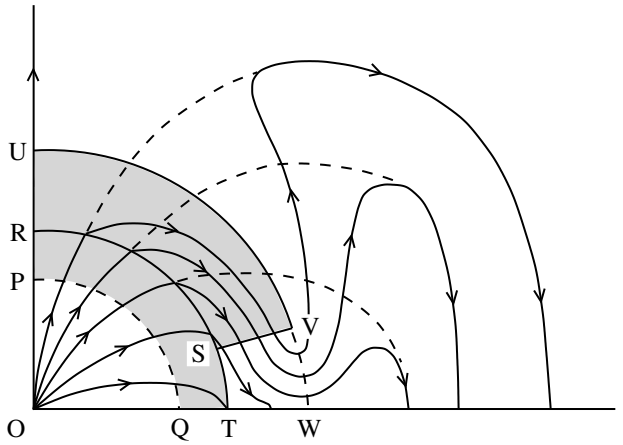

Figure 1 Schematic diagram (not to scale) of the magnetic field of a neutron star during polar cap accretion, showing one quadrant of a meridional cross-section. *UVW* is the stellar surface after sinkage of the accreted material *UVSR*; it almost coincides with the pre-accretion surface. *RSTQP* is the original outer layer of the star, buried by the accreted overburden. *OPQ* is the undisturbed interior. The magnetic field is undistorted in *OPQ* (line tying), moderately distorted in *RSTQP*, and highly distorted in *UVSR* due to burial. The original dipole field (dashed curves) is dragged equatorward and 'trampled' beneath the leading edge *SV*, flaring out from the notch *VSTW* in a tutu-like configuration and tending to a dipole at large distances. The magnetic tension of the compressed flux in the notch *VSTW* balances the hydrostatic pressure at the base *RS* of the accreted overburden. The layer of compressed flux in *UVSR*, running nearly parallel to *UV*, is typically thinner than *UVSR*. It is located along either *UV* or *RS*, depending on the role played by Ohmic dissipation and hydromagnetic instabilities.

Litwin et al. 2001). Once more than $\sim 10^{-5} M_\odot$ of material has been accumulated (for $B_0 = 10^{12-13}$ G; see Section 2.3 and cf. Brown & Bildsten 1998; Litwin et al. 2001), the hydrostatic pressure gradient at the base of the mountain exceeds the magnetic tension of the polar flux tube, the magnetic field buckles, and the base of the mountain spreads laterally towards the equator, dragging frozen-in magnetic flux along with it.[1]

Figure 1 illustrates schematically, in cross-section, the distribution of matter and magnetic flux for $M_a \gg 10^{-5} M_\odot$. As the accreted layer *UVSR* spreads equatorward, the leading face *SV* runs over dipolar magnetic field lines (dashed curves), burying them underfoot. Magnetic flux is compressed into a narrow layer along *RS*, emerging from *SV* into the notch *VSTW*. (The notch is not evacuated in reality; it is filled by material welling up from below.) Force balance between the magnetic tension of the compressed flux and the pressure gradient at the base of *UVSR* establishes the equilibrium position of *SV*. Field lines flare outwards from the notch over a characteristic distance *ST*, becoming dipolar far from the star; the configuration resembles a ballerina's tutu. Flux conservation implies that the magnetic field strength in the notch exceeds B_0 by a factor $|RS| : |ST| \gg 1$, but the overall dipole moment of the star is *reduced* by $|ST| : |RS|$ from its original value by screening currents (Section 2.4).

The layer of compressed magnetic flux is typically thinner than *UVSR*; we show in Section 2.3 that it is $\approx 6 \times 10^2$ cm thick for $M_a = 10^{-1} M_\odot$, compared to $|SV| \approx 3 \times 10^4$ cm. A question then arises: where exactly is the flux layer located? If the leading face of *SV* runs over magnetic field lines as it moves equatorward, and if flux freezing is respected, the compressed flux must lie along *RS*. We call this buried configuration Type A. However, a Type A layer is buoyant and hence susceptible to hydromagnetic instabilities of Parker or interchange type. A full treatment of such instabilities lies outside the scope of this paper. Qualitatively, however, they act to raise the compressed flux to the surface, in the form of mushroom-like 'magnetic blisters' (Parker) or 'slabs' (interchange). We call this surface configuration Type B. In this paper, we calculate the structure of both Type A and B configurations, obtaining similar results in both cases.

The magnetic field is partially distorted in a layer of mass $\sim M_a$ beneath *UVSR*, drawn as *RSTQP* in Figure 1. Below this layer, the field is undisturbed; magnetic field lines are effectively anchored along *PQ*. This boundary condition, called line-tying, is a feature of models of magnetic loops in the solar corona (e.g. Low 1980; Zweibel & Hundhausen 1982) as well as of earlier work on accreting neutron stars (Uchida & Low 1981; Hameury et al. 1983; Brown & Bildsten 1998; Litwin et al. 2001). Note that *PQ* is not the crust–core boundary; we do not distinguish between the crust and core in this paper, nor do we model the submergence and subsequent replacement of the pre-accretion crust.

2.2 *Equations of Hydromagnetic Force Balance*

The accreted matter adjusts to hydromagnetic equilibrium on the local Alfvén time scale, $\tau_A = L/v_A \lesssim 4 \times 10^{-2}$ s, where $L \lesssim 5 \times 10^4$ cm is the thickness of the compressed flux layer (calculated *a posteriori* in Section 2.3) and $v_A = (B^2/4\pi\rho)^{1/2} \gtrsim 1 \times 10^6$ cm s^{-1} is the Alfvén speed. The Alfvén time scale is much shorter than the flow time scale, $\tau_f = 4\pi R_*^2 \rho L / \dot{M}_a \gtrsim 3 \times 10^3$ yr (Brown & Bildsten 1998), and the accretion time scale, $\tau_a = M_a/\dot{M}_a$, for $\rho = 1 \times 10^{11}$ g cm^{-3} and $\dot{M}_a = 1 \times 10^{-8} M_\odot$ yr^{-1}. Hence the spreading of the accreted matter is well described by a quasistatic sequence of hydromagnetic equilibria, provided that Ohmic dissipation is slow (Section 3.1) and the equilibria are not disrupted by hydromagnetic instabilities, e.g. Parker and interchange modes, on the time scale τ_A (Section 3.2).

The hydromagnetic structure of a neutron star in equilibrium is governed by the force equation

$$-\text{grad}\, P - \rho\, \text{grad}\, \Phi + (4\pi)^{-1} (\text{curl}\, \mathbf{B}) \times \mathbf{B} = 0. \quad (1)$$

In (1), $\mathbf{B}(\mathbf{x})$ and $\rho(\mathbf{x})$ denote the magnetic field strength and mass density respectively, the gravitational potential

[1] Litwin et al. (2001) estimate that the field buckles for $M_a \gtrsim 10^{-12} M_\odot$, the threshold depending on the ratio of the polar cap radius to the pressure scale height. However, they do not include an important effect: as the accreted material spreads equatorward, it compresses the magnetic flux outside the polar cap, increasing the external magnetic stress and stiffening the polar flux tube against significant buckling for $M_a \lesssim 10^{-5} M_\odot$ (Section 2.3).

https://doi.org/10.1071/AS01056

$\Phi(\mathbf{x})$ is determined by $\rho(\mathbf{x})$ through Poisson's equation, $\nabla^2\Phi = 4\pi G\rho$, and the scalar pressure $P(\mathbf{x})$ is related to $\rho(\mathbf{x})$ by an equation of state, taken here to be polytropic, i.e. $P = K\rho^\Gamma$. No distinction is drawn between accreted material and the original stellar material. Hydromagnetic distortion of the star occurs mainly in the outer crust, where the electrons are degenerate and relativistic yet the nucleon density is below neutron drip ($\rho < 4\times10^{11}\,\mathrm{g\,cm^{-3}}$). We therefore take $\Gamma = 1.3$ in what follows. Near neutron drip, Γ decreases sharply to $\Gamma \approx 0.35$ then rises with depth to $\Gamma \approx 1.7$ at nuclear densities (Shapiro & Teukolsky 1983, p. 196; Lai 1994). We find that our key results are insensitive to Γ.

Hydrostatic, gravitational, and Lorentz forces are included in (1). Elastic stresses developed in the crystalline outer crust are neglected. We show, *a posteriori*, that a modest amount of accretion ($M_\mathrm{a} \gtrsim 2\times10^{-3}M_\odot$; see Section 2.4) compresses the magnetic field enough to exceed locally the yield threshold $B_\mathrm{y} = 4\times10^{13}\,ZA^{-2/3}(\varepsilon/10^{-2})^{1/2}(\rho/10^{11}\,\mathrm{g\,cm^{-3}})^{2/3}\,\mathrm{G}$ (Romani 1990), above which magnetic stresses dominate elastic stresses; here, ε is the strain angle and Z and A are the charge and mass number of the crustal ions. We also neglect forces arising from superfluid, superconducting behaviour at densities above neutron drip, e.g. the Magnus force exerted on neutron vortices, which produces cyclotron–vortex waves when coupled to the Lorentz force (Mendell 1998). Neglecting such forces is justified because the magnetic field is distorted primarily in the nonsuperfluid outer crust; moreover, it can exceed $\sim10^{15}$ G locally, destroying superconductivity [fluxoid separation $\lesssim$ London depth; see Mendell 1998, equations (3) and (8)].

Let (r, θ, ϕ) be spherical polar coordinates oriented so that $\theta = 0$ defines the symmetry axis of the pre-accretion magnetic field. Then B_ϕ is zero initially. Suppose, for simplicity, that material accretes symmetrically about this axis at all times, so that there is no toroidal flow. [Basko & Sunyaev (1976) studied asymmetric accretion caused by warping of the polar flux tube when the magnetic axis is not perpendicular to the plane of the accretion disk.] Flux freezing then guarantees that $\mathbf{B}$ remains axisymmetric at all times, with $B_\phi = 0$, and there exists a scalar flux function $\psi(r,\theta)$ that generates $\mathbf{B}$ via

$$\mathbf{B} = (r\sin\theta)^{-1}\,\mathrm{grad}\,\psi(r,\theta)\times\hat{\mathbf{e}}_\phi. \tag{2}$$

We define $\psi_* = \psi(R_*, \pi/2)$ and $\psi_\mathrm{a} = \psi(R_\mathrm{a}, \pi/2)$ to be the hemispheric and polar cap fluxes respectively. Axisymmetric evolution with $B_\phi = 0$ is possible only if the pre-accretion field is purely poloidal. In reality, a toroidal field component can be generated in many ways, e.g. by a convective dynamo in the progenitor star (Thompson & Duncan 1993) or by a thermoelectric battery (Blandford et al. 1983). The accreting material is assumed to be unmagnetised, which in general is unrealistic (Uchida & Low 1981).

Upon projecting (1) along $\mathbf{B}$ and using $\mathbf{B}\cdot\mathrm{grad}\,\psi = 0$, we obtain the generalised Lane–Emden equation

$$\left[\frac{1}{r^2}\frac{\partial}{\partial r}\left(r^2\frac{\partial}{\partial r}\right) + \frac{1}{r^2\sin\theta}\frac{\partial}{\partial\theta}\left(\sin\theta\frac{\partial}{\partial\theta}\right)\right] \times\left[\left(\frac{K\Gamma}{\Gamma-1}\right)\rho^{\Gamma-1} - F(\psi)\right] + 4\pi G\rho = 0. \tag{3}$$

Upon projecting (1) along grad ψ and substituting (2), we obtain the Grad–Shafranov equation

$$4\pi\rho r^4\sin^2\theta\frac{dF(\psi)}{d\psi} + r^2\frac{\partial^2\psi}{\partial r^2} + \sin\theta\frac{\partial}{\partial\theta}\left(\frac{1}{\sin\theta}\frac{\partial\psi}{\partial\theta}\right) = 0. \tag{4}$$

To calculate the equilibrium state, one needs to solve (3) and (4) simultaneously for $\rho(r,\theta)$ and $\psi(r,\theta)$, subject to boundary conditions and a choice of the arbitrary functional $F(\psi)$.

The physical meaning of $F(\psi)$ deserves comment. Formally, $F(\psi)$ is arbitrary. In general, however, the solution of (3) and (4) with an arbitrary choice of $F(\psi)$ yields an equilibrium state that cannot be reached from our specified initial state by a continuous deformation of flux surfaces in a way that respects flux freezing and mass continuity. Indeed, for certain choices of $F(\psi)$, the sequence of equilibria terminates when M_a increases beyond a critical value; no solution of the prescribed form exists, and there is a loss of equilibrium (Klimchuk & Sturrock 1989 give a force-free example). This happens because (1) does not contain the evolutionary information in the induction and mass continuity equations. A supplementary constraint on the mass-to-flux ratio does fix $F(\psi)$ uniquely: one solves (3) and (4) subject to the condition (Mouschovias 1974; Shu 1992, p. 320)

$$2\pi\int_C\frac{ds\,\rho[r(s),\theta(s)]}{|\mathbf{B}[r(s),\theta(s)]|} = \begin{cases}(dM/d\psi)_0 + M_\mathrm{a}/\psi_\mathrm{a} & \text{for } 0\le\psi\le\psi_\mathrm{a}\\ (dM/d\psi)_0 & \text{for } \psi\ge\psi_\mathrm{a}\end{cases}, \tag{5}$$

where C is the curve $\psi[r(s),\theta(s)] = \psi$, $(dM/d\psi)_0$ is the mass-to-flux ratio of the spherical polytrope plus central dipole prior to accretion, and the accreted mass M_a is distributed uniformly within the polar flux tube $0\le\psi\le\psi_\mathrm{a}$. Note that the mass-to-flux constraint is not conservative in problems involving accretion.

Mouschovias (1974) sets out an iterative scheme for solving (3), (4), and (5) numerically. A full implementation of this scheme lies outside the scope of this paper and is left to future work; numerical difficulties are anticipated, because the solution features steep gradients in ρ and ψ (Section 2.3). We compromise by choosing $F(\psi)$ in such a way as to qualitatively (though not quantitatively) satisfy the mass-to-flux constraint (5) while simultaneously yielding a solution characterised by equatorward

hydromagnetic spreading as M_a increases. Our particular choice,

$$F(\psi) = F_0 \begin{cases} 1-(1-\psi/\psi_a)^2 & \text{for } 0 \le \psi \le \psi_a \\ 1 & \text{for } \psi \ge \psi_a \end{cases}, \quad (6)$$

where F_0 is a constant to be determined, ensures that the magnetic field is force-free ($dF/d\psi = 0$) outside the polar flux tube $0 \le \psi \le \psi_a$; flux freezing prevents accreted material from crossing flux surfaces to reach $\psi \ge \psi_a$. It is a standard procedure to guess $F(\psi)$ when modelling structures in the solar corona, e.g. prominences and arcades (Dungey 1953; Low 1980; Hundhausen, Hundhausen, & Zweibel 1981; Zweibel & Hundhausen 1982; Webb 1988; Sozou 1998), as well as accretion onto compact objects (Uchida & Low 1981; Hameury et al. 1983; Brown & Bildsten 1998; Litwin et al. 2001). Čadež, Oliver, & Ballester (1994) used an *ad hoc* pressure balance condition at a simple, fixed boundary to determine, rather than guess, $F(\psi)$.

2.3 Boundary Layer Solution

Prior to the onset of accretion, the star can be modelled as a spherical polytrope threaded by a dipolar magnetic field. Equations (3) and (4) are satisfied exactly by $\psi(r,\theta) = \psi_*(r/R_*)^{-1}\sin^2\theta$ and $\rho(r,\theta) = \rho_0 f(\tilde{r})^3$ for $M_a = 0$, where we define $\rho_0 = 13M_*/R_*^3$, $\tilde{r} = r/r_0$, and $r_0 = 0.14R_*$, and the dimensionless function $f(\tilde{r})$ satisfies the Lane–Emden equation $(\tilde{r}^2 f')' + \tilde{r}^2 f^3 = 0$, with boundary conditions $f(0) = 1$ and $f'(0) = 0$.

The above solution, which is force-free except at the (ignorable) central singularity, remains a good approximation to the exact equilibrium state once accretion commences, provided that the accreted mass is within the range $10^{-5}M_\odot \lesssim M_a \lesssim 10^{-1}M_\odot$. This is because, for $\psi \ge \psi_a$, the terms featuring $F(\psi)$ in (3) and (4), describing departures from a force-free state, are M_a/M_* times smaller than the other terms and can be neglected. However, the force-free solution is invalid for $0 \le \psi \le \psi_a$, because the first term in (4) increases to balance the second term. The terms are in the ratio $Q_a(r/\Delta r)^2$, with $Q_a = 0.25GM_*^2/\psi_a^2$, implying that the flux surfaces $0 \le \psi \le \psi_a$ are compressed within a boundary layer of thickness $\Delta r/r \propto Q_a^{-1/2} \ll 1$.

The location of the boundary layer is uncertain in the context of the present calculation, as we do not constrain the evolution through (5). Two generic possibilities are identified qualitatively in Section 2.1. In a Type A configuration, the boundary layer lies along *RS* in Figure 1, beneath the accreted layer *UVSR*. Flux freezing is respected during the quasistatic evolution, and it is assumed that there are no disruptive hydromagnetic instabilities operating on the Alfvén time scale τ_A. In a Type B configuration, the boundary layer lies along the surface of the star, i.e. $\psi = 0$ along *UV* in Figure 1. It is assumed that Ohmic diffusion (Section 3.1) and hydromagnetic instabilities (Section 3.2) raise the compressed magnetic flux $0 \le \psi \le \psi_a$ in a stratified way. An alternative scenario — that the final state is disordered, with the compressed magnetic flux sprouting to the surface in 'blisters' — will be studied in future work. Note that the location of the buried flux layer is also uncertain in existing theories of spherical burial, which do not track instabilities on the time scale τ_A and artificially force the magnetic field to be dipolar at all times (Romani 1990; 1993; Konar & Bhattacharya 1997).

Hydromagnetic equilibria of Types A and B are constructed in Appendix A by solving (3), (4), and (6) approximately. We describe the Type B solution here by way of illustration. It has three zones. (i) Throughout most of the stellar volume, where $\psi(r,\theta) \ge \psi_a$, we find $\psi(r,\theta) = \psi_*(r/R_*)^{-1}\sin^2\theta$ and $\rho(r,\theta) = \rho_0[f(\tilde{r}) + \delta_a]^3$, with $\delta_a = 0.15M_a/M_*$. (ii) In the boundary layer $0 \le \psi(r,\theta) \le \psi_a$, whose thickness L is given by $L/R_* = 0.021Q_a^{-1/2}\delta_a^{-2}$, we find

$$\psi(r,\theta) = 2^{-1/2}\psi_a(L/R_*)^{-1}(1-r/R_*)\sin\theta, \quad (7)$$

$$\rho(r,\theta) = \rho_0\delta_a^3[1-(1-\psi/\psi_a)^2]^3, \quad (8)$$

a good approximation for $\psi \ll \psi_a$ and wherever the $\partial/\partial\theta$ terms in (4) can be ignored. (iii) Near $\theta = \pi/2$, where the $\partial/\partial\theta$ terms are significant, a second boundary layer forms, of characteristic dimensions $\Delta r = L$ and $\Delta\theta = 0.14L/R_*$, enabling (7) to match smoothly to $\psi(R_*, \pi/2) = \psi_*$ and $\rho(R_*, \pi/2) = \rho_0\delta_a^3$. The magnetic flux surfaces $\psi_a \le \psi \le \psi_*$ are magnetically disconnected from the accretion disk and free of accreted material. Note that the solutions in zones (i)–(iii) join together semi-quantitatively but not exactly; it is hard to solve (3) and (4) analytically with a free boundary (Biskamp 1993), and a numerical solution is deferred to future work. A restricted, linear version of the problem — where the gravitational potential is imposed, not derived from ρ — was solved with Cauchy (line-tying) boundary conditions by Uchida & Low (1981). A boundary layer treatment of unmagnetised accretion and spreading, including rotation and radiation effects, was carried out by Inogamov & Sunyaev (1999).

An order of magnitude estimate of the thickness L of the boundary layer can be obtained as follows. If the hemispheric magnetic flux of the star, $\pi R_*^2 B_0$, is compressed into a layer of cross-sectional area $2\pi R_* L$, flux conservation implies that the field strength inside the layer (and in the notch *VSTW* in Figure 1) is $B_1 = B_0 R_*/2L$. Upon balancing the magnetic stress in the notch, $B_1^2/8\pi$, against the hydrostatic pressure at *S* in Figure 1, $GM_*M_a/2\pi R_*^4$, we obtain $L/R_* \approx 2\times 10^{-5}(M_a/10^{-2}M_\odot)^{-1/2}(B_0/10^{12.5}\,\mathrm{G})$. This reproduces exactly the scaling $L \propto (Q_a\delta_a)^{-1/2}$ corresponding to Type A equilibria (see Appendix A) and is similar to the Type B scaling $L \propto (Q_a\delta_a^4)^{-1/2}$, where the equation of state of the surface layer plays an important role.

2.4 Magnetic Dipole Moment

The external magnetic field of the star, and the magnetic dipole moment μ, are determined by the radial component

https://doi.org/10.1071/AS01056

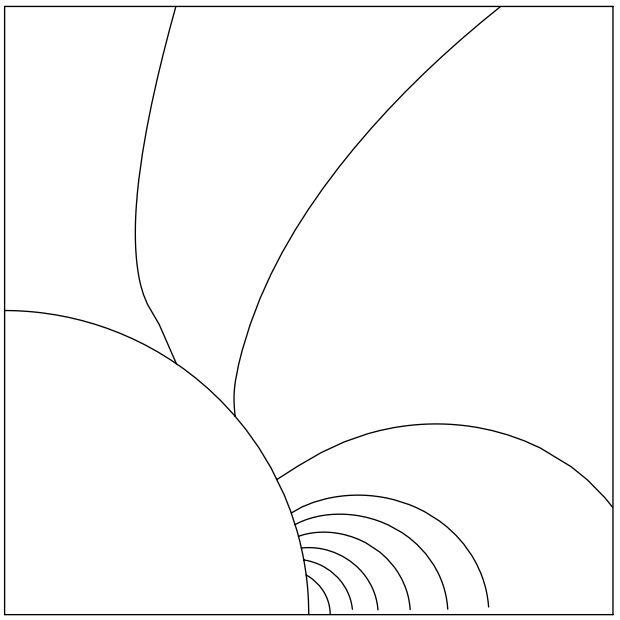

Figure 2 Equatorial magnetic tutu of a star with $B_r(R_*,\theta) = \cos\theta/|\cos\theta|$ for $|\cos\theta| \le 0.3$, and $B_r(R_*,\theta) = 0$ for $0.3 < |\cos\theta| \le 1$. The magnetic field lines correspond to field strengths $\eta|\mathbf{B}(R_*,\pi/2)|$, $\eta = 0.1, 0.2, \ldots, 0.9$, ordered from pole to equator. Multipoles $l \le 15$ are summed when calculating the field.

of the magnetic field at the stellar surface:

$$\mu = \frac{3}{4}R_*^3 \int_{-1}^{1} d(\cos\theta)\ \cos\theta\ B_r(R_*,\theta). \tag{9}$$

We assume that currents are negligible in the region $r \ge R_*$, so that the external field is potential. It is clear from (7) that $B_r(R_*,\theta)$ is zero for $|\pi/2-\theta| > L/R_*$ and is large in the equatorial notch $|\pi/2-\theta| < L/R_*$, where one has $B_r \approx \pm 6.9\psi_* R_*^{-1} L^{-1}$, with the positive and negative signs corresponding to the northern and southern hemispheres respectively. The resulting external field is plotted in Figure 2 for the test case $L/R_* = 0.3$, corresponding to $M_a/M_* = 3.8\times10^{-3}(B_0/10^{12.5}\,\mathrm{G})^{1/2}(\psi_a/\psi_*)^{1/2}$. The field geometry is distinctive, resembling the flaring tutu of a ballerina in cross-section, with the flux near the stellar surface concentrated in an equatorial band. For the Type B configuration, (7) and (9) lead to

$$\mu = 6.6\times10^{23}\left(\frac{\psi_a}{\psi_*}\right)\left(\frac{M_a}{M_*}\right)^{-2}\left(\frac{B_0}{10^{12.5}\,\mathrm{G}}\right)^2 \mathrm{G\,cm^3}. \tag{10}$$

A similar result, with $\mu \propto M_a^{-1/2}$ and the same order of magnitude, is obtained for the Type A configuration; see Appendix A.

The magnetic dipole moment decreases as more material accretes, even though the surface magnetic field at the equator increases. This is because μ is dominated by the surface magnetic field at the poles, which is buried in the above scenario; μ therefore decreases by the weighting factor $\cos\theta \sim L/R_*$. Note that, in the notch *VSTW* in Figure 1, the magnetic field $B_r \approx 22$ $(L/R_*)^{-1}B_0$ is much greater than the original polar field, although much less than the virial field 4×10^{18} G (Lai & Shapiro 1991) for realistic amounts of accreted material $M_a \lesssim M_\odot$. Even a modest amount of accretion ($M_a \gtrsim 2\times10^{-3}M_\odot$) compresses the magnetic field enough to locally exceed the yield value $B_y = 4\times10^{13}\,Z\,A^{-2/3}(\varepsilon/10^{-2})^{1/2}(\rho/10^{11}\,\mathrm{g\,cm^{-3}})^{2/3}$ G (Romani 1990), above which magnetic stresses dominate elastic stresses, justifying our neglect of elastic stresses in (1).

2.5 Mass Quadrupole Moment

Matter is distributed asymmetrically in the compressed flux layer. $\psi(r,\theta)$ varies as a function of θ through (7), and the associated hydromagnetic stresses induce a conjugate variation in $\rho(r,\theta)$ to satisfy (1). For a magnetic field of the form (2), the star is biaxial, with principal moments of inertia $I_1 = I_2 < I_3$, and principal axis $\mathbf{e}_1$ directed along the pre-accretion magnetic dipole $\mathbf{m}$. The ellipticity of the star, $\epsilon = (I_1 - I_3)/I_1$, is then given by

$$\epsilon = \pi I_0^{-1}\int_{-1}^{1} d(\cos\theta)\int_0^{R_*} dr\, r^4(3\cos^2\theta - 1)\rho(r,\theta) \tag{11}$$

$$= 8.0\times10^{-6}\left(\frac{\psi_a}{\psi_*}\right)\left(\frac{M_a}{M_*}\right)\left(\frac{B_0}{10^{12.5}\,\mathrm{G}}\right) \tag{12}$$

for the Type B configuration, where I_0 is the moment of inertia of the undistorted star, and (12) is obtained from (11) using (7) and (8). (The contribution to ϵ of the notch *VSTW* is smaller by a factor $\sim L/R_*$ and can be neglected.) An analogous result for the Type A configuration follows from (11), (A9), and (A10) and depends on the depth as well as the thickness of the flux layer.

2.6 Dependence on $\dot{M}_a$

The magnetic dipole moment μ is proportional to the polar magnetic flux, $\psi_a \propto R_a^{-1}$, which is itself a function of μ through R_a. In the Ghosh & Lamb (1979) model of the magnetosphere of an accreting neutron star, the inner disk boundary at R_a is located where the magnetic stress of the stellar dipole ($\propto \mu^2$) balances the inward ram pressure of the disk ($\propto \dot{M}_a$), viz.

$$R_a/R_* = \left(8\mu^4/GM_*R_*^7\dot{M}_a^2\right)^{1/7} \tag{13}$$

$$= 2.7\times10^2\left(\frac{\mu}{10^{30}\,\mathrm{G\,cm^3}}\right)^{4/7} \times\left(\frac{\dot{M}_a}{10^{-8}\,M_\odot\,\mathrm{yr^{-1}}}\right)^{-2/7}. \tag{14}$$

Upon combining (14) with (10), using $\psi_a/\psi_* = R_*/R_a$, we can solve for μ to obtain

$$\frac{\mu}{10^{30}\,\mathrm{G\,cm^3}} = 5.2\times10^{-6}\left(\frac{\dot{M}_a}{10^{-8}\,M_\odot\,\mathrm{yr^{-1}}}\right)^{2/11} \times\left(\frac{M_a}{M_\odot}\right)^{-14/11}\left(\frac{B_0}{10^{12.5}\,\mathrm{G}}\right)^{14/11}, \tag{15}$$

$$\frac{\psi_a}{\psi_*} = 3.9 \left(\frac{\dot{M}_a}{10^{-8}\, M_\odot\, \mathrm{yr}^{-1}} \right)^{2/11} \times \left(\frac{M_a}{M_\odot} \right)^{8/11} \left(\frac{B_0}{10^{12.5}\, \mathrm{G}} \right)^{-8/11}, \quad (16)$$

and hence, from (12) and (16),

$$\epsilon = 2.1 \times 10^{-5} \left(\frac{\dot{M}_a}{10^{-8}\, M_\odot\, \mathrm{yr}^{-1}} \right)^{2/11} \times \left(\frac{M_a}{M_\odot} \right)^{19/11} \left(\frac{B_0}{10^{12.5}\, \mathrm{G}} \right)^{3/11}. \quad (17)$$

Note that μ and ϵ depend weakly on $\dot{M}_a$. The coefficients of proportionality in (15) and (17) also depend weakly on the (uncertain) details of the magnetospheric geometry, which determine the exact value of R_a.

3 Nonideal Magnetic Field Evolution

In this section, we assess critically the key assumptions underlying the theory in Section 2, namely that magnetic flux freezing is continuously respected as equatorward spreading proceeds, and that the hydromagnetic configuration of the star evolves through a quasistatic sequence of equilibria. Ohmic dissipation is incorporated into the theory semiquantitatively in Section 3.1, and the existence of Parker-type instabilities is discussed in Section 3.2. Both effects tend to limit the effectiveness of spreading and burial. Section 3.3 compares the approach in this paper with previous models of field burial.

3.1 Ohmic Dissipation

The results in Section 2 are derived on the basis that the accreted material is perfectly conducting. In reality, the surface layers of a neutron star are resistive, due to electron–phonon and electron–impurity scattering (e.g. Brown & Bildsten 1998). Ohmic dissipation therefore modifies the process of equatorward hydromagnetic spreading.

A magnetic flux tube of characteristic dimension L' dissipates on the Ohmic time scale $\tau_d = 4\pi\sigma L'^2/c^2$, where $\sigma = (Z\rho e^2/Am_p m_e)(1+x^2)^{-1/2}(\nu_{ph}+\nu_{imp})^{-1}$ is the electrical conductivity, $\nu_{ph} = (\hbar^2 c/13e^2 k_B T)^{-1}[1 + (\Theta/3.5T)^2]^{-1/2}$ and $\nu_{imp} = (3\pi\hbar^3 Z/8m_e e^4 Q x)^{-1}$ are the electron–phonon and electron–impurity collision frequencies, $x = p_F/m_e c = 1.0(Z/A)^{1/3}(\rho/10^6\ \mathrm{g\ cm^{-3}})^{1/3}$ is the dimensionless Fermi momentum, and Q measures the impurity concentration (Brown & Bildsten 1998). If τ_d is greater than the flow time scale, $\tau_f = 4\pi R_*^2 \rho L'/\dot{M}_a$, then, to a good approximation, magnetic field lines are frozen into the fluid on the length scale L'. If τ_d is less than τ_f, magnetic field lines diffuse through the fluid. Brown & Bildsten (1998) compared τ_d and τ_f across a pressure scale height h and found $\tau_d/\tau_f \approx \dot{M}_a/(2\times10^{-7} M_\odot\ \mathrm{yr}^{-1})$. The ratio is approximately independent of density, because we have $L' = h \propto \rho^{1/3}$, $\sigma \propto \rho(x\nu_{ph})^{-1} \propto \rho^{2/3}$, and hence $\tau_d \propto \tau_f \propto \rho^{4/3}$. However, it is shown in Section 2.3 that the compressed flux layer is much thinner than the pressure scale height, with $L \lesssim 6\times10^2$ cm and $h \approx 5\times10^4$ cm for $M_a \gtrsim 10^{-5} M_\odot$. Upon revising the estimate of Brown & Bildsten (1998) to apply to the compressed flux layer, we find $\tau_d = 1.4\times10^{14}(L/R_*)^2$ s versus $\tau_f = 2.0\times10^{12}(L/R_*)(\dot{M}_a/10^{-8}M_\odot\ \mathrm{yr}^{-1})^{-1}$ s for conditions at the base of the outer crust, viz. $\rho = 1\times10^{11}\ \mathrm{g\ cm^{-3}}$, $T = 3\times10^8$ K, $A = 2Z = 12$, $x = 37$, $\Theta = 5.6\times10^8$ K, $\nu_{ph} = 3.3\times10^{18}\ \mathrm{s^{-1}}$, $\nu_{imp} = 2.1\times10^{17}\mathrm{s^{-1}}$, and $\sigma = 9.7\times10^{21}\ \mathrm{s^{-1}}$.

How does Ohmic dissipation modify the process of equatorward hydromagnetic spreading? Magnetic field lines diffuse through the fluid over distances less than $L_d = 1.4\times10^{-2}(\dot{M}_a/10^{-8}\ M_\odot\ \mathrm{yr}^{-1})^{-1} R_*$, the length scale where one has $\tau_d = \tau_f$. Therefore L_d is the minimum width of the equatorial tutu. It is attained when $M_a/M_* \geq 1.7\times10^{-2}(\dot{M}_a/10^{-8}\ M_\odot\ \mathrm{yr}^{-1})^{1/2}(B_0/10^{12.5}\ \mathrm{G})^{1/2}(\psi_a/\psi_*)^{1/2}$ and implies a minimum magnetic moment

$$\mu_{min} = 2.4\times10^{27} \left(\frac{\dot{M}_a}{10^{-8}\, M_\odot\, \mathrm{yr}^{-1}} \right)^{-1} \times \left(\frac{B_0}{10^{12.5}\, \mathrm{G}} \right) \mathrm{G\ cm^3} \quad (18)$$

and a maximum ellipticity

$$\epsilon_{max} = 1.3\times10^{-7} \left(\frac{\psi_a}{\psi_*} \right)^{3/2} \times \left(\frac{\dot{M}_a}{10^{-8}\, M_\odot\, \mathrm{yr}^{-1}} \right)^{1/2} \left(\frac{B_0}{10^{12.5}\, \mathrm{G}} \right)^{3/2} \quad (19)$$

from (10) and (12) respectively, independent of chemical composition to a first approximation ($\nu_{ph} \gg \nu_{imp}$; cf. Konar & Bhattacharya 1997, 1998). After accretion shuts off, the magnetic field in the tutu and buried flux layer is likely to diffuse poleward and resurface, with a concomitant increase in μ. The time scale for poleward diffusion, $\tau_d = 1.4\times10^{14}(L/R_*)^2$ s, lengthens progressively as diffusion proceeds and the gradient scale L increases. For $\tau_d \lesssim 10^7$ yr, i.e. $L \lesssim R_*$, the pre-accretion μ is partially restored. More work is required to determine whether μ is fully restored in older objects.

In a recent paper, Cumming et al. (2001) improved upon the semiquantitative estimates (18) and (19) by constructing exact hydromagnetic equilibria illustrating the competition between Ohmic dissipation and burial by accretion. They found burial to be effective for $\dot{M}_a \gtrsim 2\times10^{-9}\ M_\odot\ \mathrm{yr}^{-1}$, although the field resurfaces $\lesssim 10^3$ yr after accretion halts and may be disrupted by buoyancy and thermomagnetic instabilities (Section 3.2). However, these conclusions do not transfer directly to the problem considered here, as they are derived for a plane parallel geometry where the magnetic tension force vanishes and one has $L \sim h$.

3.2 Hydromagnetic Instabilities

The equilibria constructed in Sections 2.2 and 2.3 are implicitly assumed to be stable for all M_a. However, in

the late stages of accretion, when the magnetic field is highly distorted as in Figures 1 and 2, the equilibria are potentially unstable on the Alfvén time scale $\tau_{\rm A}$, breaking the quasistatic sequence. This is especially true when the mass-to-flux ratio is not constrained through (5); Mouschovias (1974) argued (by example) that an iterative numerical scheme that solves (3) and (4) will converge to a stable state only if supplemented by (5).

In the Type A configuration, the buoyancy of the compressed magnetic flux (light fluid) along RS in Figure 1 can drive long-wavelength, slow MHD modes that overturn the accreted overburden (heavy fluid) on the time scale $\tau_{\rm A}$. Magnetic field lines arch upward out of the surface, forming 'magnetic blisters', while the accreted material slides downward along field lines and collects in 'magnetic valleys'. The final state is likely to be disordered. This process is analogous to the global Rayleigh–Taylor instability of the Galactic magnetic field discovered by Parker (1966). However, it is difficult to be sure that the instability proceeds, because the equilibrium state for $M_{\rm a} \gtrsim 10^{-5} M_\odot$ has not yet been calculated rigorously. There are hints that the configuration is poised on the edge of instability, with the outcome depending sensitively on geometry. For example, Parker's (1966) instability criterion for a plane parallel flux layer (cf. RS),

$$(1+\alpha)(\alpha - \Gamma + 1) - \alpha\Gamma/2 > 0, \qquad (20)$$

where $\alpha = B^2/8\pi P$ is uniform in the equilibrium state, borders on being satisfied (or violated) given $\alpha \sim 1$ in the vicinity of RS. Equation (20) is a global criterion and cannot be applied locally to RS without modification; nevertheless, it is suggestive. In addition, the Parker instability may be quenched prematurely, as magnetic field lines arch upward and α decreases locally to $\alpha \ll 1$. An accurately calculated equilibrium state is necessary before a definitive conclusion about stability can be reached.

Litwin et al. (2001) showed, on the basis of an MHD energy principle, that short-wavelength ballooning modes with line-tying boundary conditions are unstable for $\alpha \lesssim 0.1(R_{\rm a}/R_*)^{1/2} h/R_*$, i.e. for $M_{\rm a} \gtrsim 10^{-12} M_\odot$. They did not address whether the nonlinear growth of the unstable modes is inhibited, e.g. by line-tying, and they analysed an equilibrium state that exists only for small field-line distortions (cf. Figure 1). Cumming et al. (2001) analysed a plane parallel geometry and showed that the layer is disrupted by buoyancy and interchange instabilities for $B \gtrsim 10^{10}$ G and by a diffusive, thermomagnetic instability for $B \gtrsim 10^{11}$ G and $\dot{M}_{\rm a} = 2 \times 10^{-7}\, M_\odot\ {\rm yr}^{-1}$. They too neglected spherical geometry and the effect of line-tying on nonlinear growth. Instabilities of the kinds discussed above are modified by nonideal MHD effects that operate on time scales longer than $\tau_{\rm A}$, e.g. superconducting Hall drift (Urpin & Shalybkov 1999).

We estimate μ and ϵ for the two extreme scenarios where hydromagnetic instabilities do (Type B) and do not (Type A) occur in Appendix A, deferring the more complicated scenario of a partially buried, disordered magnetic field to future work. We emphasise that the geometry and location of the buried flux layer, and hence μ, are equally uncertain in spherical models of burial (Romani 1990; 1993; Konar & Bhattacharya 1997), which do not resolve the time scale $\tau_{\rm A}$ and artificially inhibit Parker-like instabilities by prescribing a spherical density profile and dipolar magnetic field.

3.3 *Comparison with Other Treatments of Magnetic Burial*

Most existing calculations of magnetic burial prescribe a spherically symmetric density distribution $\rho(r)$ and a magnetic field of the quasi-dipolar form $\mathbf{B} = {\rm curl}\,[r^{-1} g(r,t) \sin\theta\, \mathbf{e}_\phi]$, where $g(r,t)$ satisfies the induction equation (Romani 1990; 1993; Urpin & Geppert 1995; Konar & Bhattacharya 1997, 1998)

$$\frac{\partial g(r,t)}{\partial t} = v(r)\frac{\partial g(r,t)}{\partial r} + \frac{c^2}{4\pi\sigma}\left[\frac{\partial^2 g(r,t)}{\partial r^2} - \frac{2g(r,t)}{r^2}\right], \qquad (21)$$

The radial velocity profile $v(r)$ is also prescribed: two common choices are $v(r) = 0$ (Romani 1990; 1993) and $v(r) = \dot{M}_{\rm a}/4\pi r^2 \rho(r)$ (Konar & Bhattacharya 1997, 1998). In contrast, the theory in Section 2 allows high-order multipoles to develop and determines both $\rho(r,\theta)$ and $\psi(r,\theta)$ self-consistently from (3) and (4), while assuming $v(r) = 0$ as in earlier work and neglecting Ohmic dissipation. Sahrling (1998) included $\partial/\partial\theta$ terms in (21), obtaining high-order multipoles of significant amplitude, but prescribed $\rho(r)$. Cheng & Zhang (1998) noted that the polar cap expands as material is added, dragging magnetic field lines equatorward, but ignored the back reaction exerted by hydromagnetic stresses.

Some authors have studied the nondipolar outcome of polar cap accretion by solving the Grad–Shafranov problem, formulated in Section 2.2, for a magnetostatic mountain of accreted material confined by magnetic stresses in the polar flux tube (Uchida & Low 1981; Hameury et al. 1983; Brown & Bildsten 1998; Litwin et al. 2001). None of this work incorporates the mass-to-flux constraint (5), a weakness shared by the approximate solutions in Appendix A. In addition, the associated numerical calculations are restricted to the regime $M_{\rm a} \lesssim 10^{-12} M_\odot$, where field-line distortion is modest and μ is reduced by a factor of order unity at most. This does not describe the late stage of accretion, $M_{\rm a} \gtrsim 10^{-2} M_\odot$ (see Figure 1). Ohmic dissipation is neglected.

Uchida & Low (1981) treated the scenario where the accreting plasma is magnetised. They found that the topology of the buried magnetic field depends on whether the accreting plasma is magnetised (anti)parallel to the intrinsic magnetic moment of the star: in the parallel case, the equator is an X-type neutral ring; in the antiparallel case, the original dipole field is compressed quasi-spherically and material drains along field lines to form a disk in the equatorial plane. The volume of closed field lines decreases with $M_{\rm a}$ in both cases. Solutions

https://doi.org/10.1071/AS01056

of the form $\psi(r,\theta) \propto \sin^2\theta$ are assumed, artificially suppressing high-order multipoles.

Time-dependent, resistive-MHD simulations of quasi-spherical, superAlfvénic accretion onto a magnetic dipole were carried out recently by Toropin et al. (1999), to study the global structure of the inflow. An expanding shock wave forms near the Alfvén surface. The flow inside the shock is subAlfvénic and collimated by the polar flux tube, and a stagnation torus forms in the equator. Screening currents reduce μ outside the shock. The parameter regime and boundary conditions (superconducting equatorial disk with a fixed ring current) do not apply directly to an accreting neutron star, but the magnetospheric shock and reduced μ are likely to be generic features.

Acknowledgments

This work was supported by NASA Grants NAG5–2756 and NAG5–3073, NSF Grants AST–93–15455 and AST–95–28271, and by the Miller Institute for Basic Research in Science through a Miller Fellowship.

A Approximate Analytic Solution of the Grad–Shafranov Equation for $10^{-5}M_\odot \lesssim M_a \lesssim 10^{-1}M_\odot$

In this appendix, we solve equations (3), (4), and (6) by a modified version of the technique of matched asymptotic expansions, in the regime $10^{-5}M_\odot \lesssim M_a \lesssim 10^{-1}M_\odot$ where accretion compresses the magnetic field of the star into a thin boundary layer.

We define dimensionless variables $\tilde\rho = (\rho/\rho_0)^{1/n}$, $\tilde\psi = \psi/\psi_a$, $\tilde r = r/r_0$, and $\tilde\mu = \cos\theta$, where $\rho_0 = 13M_*/R_*^3$ and $r_0 = 0.14R_*$ are the central density and radial scale of a spherical, $\Gamma = 1.3$ polytrope, and ψ_a is the magnetic flux enclosed by the inner edge of the accretion disk at $r = R_a$ (Ghosh & Lamb 1979; Basko & Sunyaev 1976). In terms of the new variables, with $F_0 = 4\pi G\rho_0 r_0^2\delta_a$, (3), (4), and (6) take the form

$$\tilde\nabla^2\tilde\rho + \tilde\rho^3 - \delta_a\tilde\nabla^2\tilde F(\tilde\psi) = 0, \tag{A1}$$

$$\tilde\Delta^2\tilde\psi + Q_a\delta_a\tilde\rho^3\tilde r^2\tilde F'(\tilde\psi) = 0, \tag{A2}$$

$$\tilde F(\tilde\psi) = \begin{cases} 1-(1-\tilde\psi)^2 & \text{for } 0\le\tilde\psi\le 1 \\ 1 & \text{for } \tilde\psi \ge 1 \end{cases}, \tag{A3}$$

with the definitions

$$\tilde\nabla^2 = \tilde r^{-2}\frac{\partial}{\partial\tilde r}\left(\tilde r^2\frac{\partial}{\partial\tilde r}\right) + \tilde r^{-2}\frac{\partial}{\partial\tilde\mu}\left[(1-\tilde\mu^2)\frac{\partial}{\partial\tilde\mu}\right], \tag{A4}$$

$$\tilde\Delta^2 = (1-\tilde\mu^2)^{-1}\frac{\partial^2}{\partial\tilde r^2} + \tilde r^{-2}\frac{\partial^2}{\partial\tilde\mu^2}, \tag{A5}$$

$Q_a = (4\pi)^2 G\rho_0^2 r_0^6/\psi_a^2 = 0.25GM_*^2/\psi_a^2$, and $\delta_a = -1 + \int d^3\tilde{\mathbf{x}}\,\tilde\rho = 0.15M_a/M_*$ [using (A14)]. In the regime $10^{-5}M_\odot \lesssim M_a \lesssim 10^{-1}M_\odot$, one has $\delta_a \ll 1$ and $Q_a\delta_a \gg 1$. In the limit $M_a \to 0$, (A1) and (A2) describe a spherical polytrope ($\tilde\nabla^2\tilde\rho + \tilde\rho^3 = 0$) and force-free magnetic field ($\tilde\Delta^2\tilde\psi = 0$).

The magnetic field is distorted near the stellar surface, where one has $\tilde\rho \ll 1$ (e.g. $\tilde\rho \approx 0.1$ beneath $10^{-2}M_\odot$ of accreted material). It is compressed into a layer much thinner than the accreted layer (verified *a posteriori*). We therefore have $\tilde\nabla^2\tilde\rho \gg \tilde\rho \gg \tilde\rho^3$ and can solve (A1) approximately to obtain

$$\tilde\rho(\tilde r,\tilde\mu) = f(\tilde r) + \delta_a\tilde F[\tilde\psi(\tilde r,\tilde\mu)]. \tag{A6}$$

The dimensionless function $f(\tilde r)$ satisfies the Lane–Emden equation $(\tilde r^2 f')' + \tilde r^2 f^3 = 0$, with boundary conditions $f(0) = 1$ and $f'(0) = 0$, and is given approximately by $f(\tilde r) \approx 0.29(\tilde r_*/\tilde r - 1)$ for $f \ll 1$. We can add to (A6) any harmonic function that satisfies the boundary conditions.

A.1 Type A Equilibria

If flux freezing is respected throughout the burial process, and if the system is stable to Parker and interchange modes (Section 3.2), the buried flux lies along *RS* in Figure 1; the leading face *SV* of the accreting material spreads equatorward and 'tramples' magnetic field lines underfoot. The layer is located at $\tilde r_c = \tilde r_*[1-(M_a/M_*)^{0.25}]^{-1} \approx \tilde r_*$, implying $f(\tilde r_c) = 0.29(M_a/M_*)^{0.25}[1-(M_a/M_*)^{0.25}]^{-1} \gg \delta_a\tilde F(\tilde\psi)$ and hence, from (A2) and (A6),

$$\tilde\Delta^2\tilde\psi + Q_a\delta_a[f(\tilde r_c)]^3\tilde r_c^2\tilde F'(\tilde\psi) = 0. \tag{A7}$$

We solve (A7) subject to two boundary conditions: (i) $\tilde\psi(\tilde r,\tilde\mu \ne 0) \to \tilde r^{-1}(1-\tilde\mu^2)$ at the inner edge of the boundary layer, where the original dipole field is undisturbed (line-tying), and (ii) $\tilde\psi(\tilde r_*, 0) = \tilde\psi_*$, because material does not accrete onto closed field lines.

In the boundary layer, we have $\partial^2/\partial\tilde r^2 \gg \partial^2/\partial\tilde\mu^2$ except near $\tilde\mu = 0$. Upon defining a stretched radial coordinate x, such that $\tilde r = \tilde r_c(1-ax)$ and $a = L/R_c = (Q_a\delta_a)^{-1/2}[f(\tilde r_c)]^{-3/2}\tilde r_c^{-2} \ll 1$, substituting into (A7), and retaining terms of lowest order in a, we obtain $\partial^2\tilde\psi/\partial x^2 + (1-\tilde\mu^2)\tilde F'(\tilde\psi) = 0$, which can be integrated subject to the boundary conditions $\partial\tilde\psi/\partial x \to 0$, $\tilde\psi \to 1$ as $x \to \infty$ (asymptotic matching) to yield

$$\int_0^{\tilde\psi} d\tilde\psi'\,[1-\tilde F(\tilde\psi')]^{-1/2} = [2(1-\tilde\mu^2)]^{1/2}x. \tag{A8}$$

We solve (A3) and (A8) numerically and find that the solution is approximated to an accuracy of 20 per cent by

$$\tilde\psi = \begin{cases} [2(1-\tilde\mu^2)]^{1/2}x & \text{for } 0 \le x \le [2(1-\tilde\mu^2)]^{-1/2} \\ 1 & \text{for } x \ge [2(1-\tilde\mu^2)]^{-1/2} \end{cases}, \tag{A9}$$

$$\tilde\rho = f(\tilde r) + \delta_a\tilde F(\tilde\psi). \tag{A10}$$

The solution exhibits the following properties: $\tilde\psi(\tilde r_*, 1) = 0$, as required by east–west symmetry, $\tilde\psi$ is an even function of $\tilde\mu$, as required by north–south symmetry, and $\tilde\psi \to 0$ at a finite radius, $\tilde r_c$.

Near $\tilde{\mu}=0$, we have $\partial^2/\partial\tilde{r}^2 \sim \partial^2/\partial\tilde{\mu}^2$, as $\tilde{\psi}$ increases smoothly from $\tilde{\psi}\leq 1$ to $\tilde{\psi}=\tilde{\psi}_* \gg 1$, and (A9) and (A10) are invalid. A second boundary layer is required at $\tilde{\mu}=0$, of characteristic latitudinal extent $\Delta\tilde{\mu}=-a/\tilde{r}_c$. Its structure can be determined by solving (A7) with full Cauchy boundary conditions. We do not attempt this here, because a semiquantitative estimate of $\Delta\tilde{\mu}$ suffices for calculating the magnetic dipole moment of the star in Section 2.4.

A.2 Type B Equilibria

If the system is unstable to Parker or interchange modes (Section 3.2), the magnetic field rises to the surface on the time scale τ_A. If the instability evolves in a stratified manner, the buried flux settles along UV in Figure 1, implying $f(\tilde{r}) \ll \delta_a \tilde{F}(\tilde{\psi})$ and hence, from (A2) and (A6),

$$\tilde{\Delta}^2\tilde{\psi} + Q_a\delta_a^4[\tilde{F}(\tilde{\psi})]^3\tilde{r}^2\tilde{F}'(\tilde{\psi}) = 0. \qquad \text{(A11)}$$

A study of the more complicated scenario of disordered evolution (e.g. magnetic blisters) is deferred to future work.

Upon defining a stretched radial coordinate y, such that $\tilde{r}=\tilde{r}_*(1-by)$ with $b=L/R_*=(Q_a\delta_a^4\tilde{r}_*^4)^{-1/2}$, and proceeding as for Type A, we find $\partial^2\tilde{\psi}/\partial y^2 + (1-\tilde{\mu}^2)[\tilde{F}(\tilde{\psi})]^3\tilde{F}'(\tilde{\psi})=0$, which can be integrated to yield

$$\int_0^{\tilde{\psi}} d\tilde{\psi}'\,[1-\tilde{F}(\tilde{\psi}')^4]^{-1/2} = [(1-\tilde{\mu}^2)/2]^{1/2}y, \quad \text{(A12)}$$

with approximate solution

$$\tilde{\psi} = \begin{cases} [(1-\tilde{\mu}^2)/2]^{1/2}y & \text{for } 0\leq y\leq[(1-\tilde{\mu}^2)/2]^{-1/2} \\ 1 & \text{for } y\geq[(1-\tilde{\mu}^2)/2]^{-1/2} \end{cases}, \qquad \text{(A13)}$$

$$\tilde{\rho} = f(\tilde{r}) + \delta_a\tilde{F}(\tilde{\psi}). \qquad \text{(A14)}$$

Equations (A13) and (A14) reduce to (7) and (8) when reexpressed in dimensional variables. A second boundary layer exists at $\tilde{\mu}=0$, of characteristic latitudinal extent $\Delta\tilde{\mu}=-b/\tilde{r}_*$, as for Type A equilibria.

References

Arons, J., & Lea, S. M. 1980, ApJ, 235, 1016
Basko, M. M., & Sunyaev, R. A. 1976, Soviet Ast., 20, 537
Bhattacharya, D., & Srinivasan, G. 1995, in X-Ray Binaries, eds W. H. G. Lewin, J. van Paradijs, & E. P. J. van den Heuvel (Cambridge: Cambridge University Press), 495
Bhattacharya, D., Wijers, R. A. M. J., Hartman, J. W., & Verbunt, F. 1992, A&A, 254, 198
Biskamp, D. 1993, Nonlinear Magnetohydrodynamics (Cambridge: Cambridge University Press)
Blandford, R. D., Applegate, J. H., & Hernquist, L. 1983, MNRAS, 204, 1025
Blandford, R. D., de Campli, W. M., & Königl, A. 1979, Bull. Am. Astron. Soc., 11, 703
Blondin, J. M., & Freese, K. 1986, Nature, 323, 786
Brown, E. F., & Bildsten, L. 1998, ApJ, 496, 915
Burderi, L., King, A. R., & Wynn, G. A. 1996, MNRAS, 283, L63
Čadež, V. M., Oliver, R., & Ballester, J. L. 1994, A&A, 282, 934
Chakrabarty, D., & Morgan, E. H. 1998, Nature, 394, 346
Chen, K., Ruderman, M., & Zhu, T. 1998, ApJ, 493, 397
Cheng, K. S., & Dai, Z. G. 1997, ApJ, 476, L39
Cheng, K. S., & Zhang, C. M. 1998, A&A, 337, 441
Cumming, A., Zweibel, E., & Bildsten, L. 2001, ApJ, submitted (astro-ph/0102178)
Dungey, J. 1953, MNRAS, 113, 180
Ghosh, P., & Lamb, F. K. 1979, ApJ, 234, 296
Hameury, J. M., Bonazzola, S., Heyvaerts, J., & Lasota, J. P. 1983, A&A, 128, 369
Hartman, J. W., Bhattacharya, D., Wijers, R., & Verbunt, F. 1997, A&A, 322, 477
Hundhausen, J. R., Hundhausen, A. J., & Zweibel, E. G. 1981, J. Geophys. Res., 86, 11117
Inogamov, N. A., & Sunyaev, R. A. 1999, Astron. Lett., 25, 269
Klimchuk, J. A., & Sturrock, P. A. 1989, ApJ, 345, 1034
Konar, S., & Bhattacharya, D. 1997, MNRAS, 284, 311
Konar, S., & Bhattacharya, D. 1998, MNRAS, 303, 588
Konar, S., & Bhattacharya, D. 1999, MNRAS, 308, 795
Kulkarni, S. R. 1986, ApJ, 306, L85
Lai, D., & Shapiro, S. L. 1991, ApJ, 383, 745
Lai, D. 1994, MNRAS, 270, 611
Litwin, C., Brown, E. F., & Rosner, R. 2001, ApJ, submitted (astro-ph/0101168)
Low, B. C. 1980, Sol. Phys., 65, 147
Melatos, A., & Phinney, E. S. 2000, in Pulsar Astronomy — 2000 and Beyond, ASP Conf. Ser., 202, eds N. Kramer, N. Wex, R. Wielebinski, 651
Mendell, G. 1998, MNRAS, 296, 903
Mouschovias, T. C. 1974, ApJ, 192, 37
Muslimov, A. G., & Tsygan, A. I. 1985, Soviet Ast. Lett., 11, 80
Parker, E. N. 1966, ApJ, 145, 811
Possenti, A., Colpi, M., D'Amico, N., & Burderi, L. 1998, ApJ, 497, L97
Romani, R. W. 1990, Nature, 347, 741
Romani, R. W. 1993, in Isolated Pulsars, eds K. A. van Riper, R. Epstein, & C. Ho (Cambridge: Cambridge University Press), 75
Ruderman, M. 1991a, ApJ, 366, 261
Ruderman, M. 1991b, ApJ, 382, 576
Sahrling, M. 1998, preprint (astro-ph/9804047)
Sang, Y., & Chanmugam, G. 1987, ApJ, 323, L61
Sengupta, S. 1998, ApJ, 501, 792
Shapiro, S. L., & Teukolsky, S. A. 1983, Black Holes, White Dwarfs, and Neutron Stars: The Physics of Compact Objects (New York: Wiley)
Shibazaki, N., Murakami, T., Shaham, J., & Nomoto, K. 1989, Nature, 342, 656
Shu, F. H., 1992, The Physics of Astrophysics. Vol. II: Gas Dynamics (Mill Valley: University Science Books)
Sozou, C. 1998, MNRAS, 295, 216
Srinivasan, G., Bhattacharya, D., Muslimov, A., & Tsygan, A. 1990, Curr. Sci., 59, 31
Taam, R. E., & van den Heuvel, E. P. J. 1986, ApJ, 305, 235
Thompson, C., & Duncan, R. C. 1993, ApJ, 408, 194
Toropin, Y. M., Toropina, O. D., Savelyev, V. V., Romanova, M. M., Chechetkin, V. M., & Lovelace, R. V. E. 1999, ApJ, 517, 906
Uchida, Y., & Low, B. C. 1981, J. Astrophys. Ast., 2, 405
Urpin, V., & Geppert, U. 1995, MNRAS, 275, 1117
Urpin, V., & Konenkov, D. 1997, MNRAS, 284, 741
Urpin, V. A., & Muslimov, A. G. 1992, MNRAS, 256, 261
Urpin, V., & Shalybkov, D. 1999, MNRAS, 304, 451
van den Heuvel, E. P. J., & Bitzaraki, O. 1995, A&A, 297, L41
Verbunt, F., Wijers, R. A. M. J., & Burm, H. 1990, A&A, 234, 195
Webb, G. M. 1988, ApJ, 327, 933
Wijers, R. A. M. J. 1997, MNRAS, 287, 607
Wijnands, R., & van der Klis, M. 1998, Nature, 394, 344
Zhang, C.-M., Wu, X.-J., & Yang, G.-C. 1994, A&A, 283, 889
Zweibel, E. G., & Hundhausen, A. J. 1982, Sol. Phys., 76, 261